Stable U(IV) complexes form at high-affinity mineral surface sites

Drew E. Latta*,[1] Bhoopesh Mishra,[2] Russell E. Cook,[3] Kenneth M. Kemner,[1] and Maxim I. Boyanov*,[1]

[1] Biosciences Division, Argonne National Laboratory, Argonne, IL 60439

[2] Physics Department, Illinois Institute of Technology, Chicago, Illinois, IL 60616

[3] Electron Microscopy Center, Argonne National Laboratory, Argonne, IL 60439

*Corresponding authors

Dr. Maxim I. Boyanov
Biosciences Division
Argonne National Laboratory
9700 South Cass Avenue, Bldg. 203
Argonne, IL 60439-4843
Phone: (630) 252-8242
Fax: (630) 252-9793
E-mail: mboyanov@anl.gov

Dr. Drew E. Latta
Biosciences Division
Argonne National Laboratory
9700 South Cass Avenue, Bldg. 203
Argonne, IL 60439-4843
Phone: (630) 252-3985
Fax: (630) 252-9793
E-mail: dlatta@anl.gov

1

2   KEYWORDS: uranium, reduction, non-uraninite products, molecular speciation

2

3   **Abstract.** Uranium (U) poses a significant contamination hazard to soils, sediments, and

4   groundwater due to its extensive use for energy production. Despite advances in modeling the

5   risks of this toxic and radioactive element, lack of information about the mechanisms controlling

6   U transport hinders further improvements, particularly in reducing environments where

7   U^{4+} predominates. Here, we establish that mineral surfaces can stabilize the majority of U as

8   adsorbed U^{4+} species following reduction of U^{6+}. Using x-ray absorption spectroscopy and

9   electron imaging analysis, we find that at low surface coverage U^{4+} forms inner-sphere

10   complexes with two metal oxides, TiO_2 and Fe_3O_4 (at <1.3 U nm^{-2} and <0.04 U nm^{-2},

11   respectively). The uraninite (UO_2) form of U^{4+} predominates only at higher surface coverage.

12   U^{4+}-TiO_2 complexes remain stable for at least 12 months and U^{4+}-Fe_3O_4 complexes remain stable

13   for at least 4 months under anoxic conditions. Adsorbed U^{4+} results from U^{6+} reduction by Fe^{2+}

14   or by the reduced electron shuttle AH_2QDS, suggesting that both abiotic and biotic reduction

15   pathways can produce stable U^{4+}-mineral complexes in the subsurface. The observed control of

16   high-affinity mineral surface sites on U^{4+} speciation helps explain the presence of non-uraninite

17   U^{4+} in sediments and has important implications for U transport modeling.

Introduction

The fate of uranium is an important consideration in the impact of energy systems on environmental quality. Long-term stewardship of spent nuclear fuel and radionuclide waste is an active issue of concern, and several countries have embarked on projects that will entomb spent fuel in geologic repositories.[1] Current environmental issues associated with uranium include releases during the Chernobyl and Fukushima Daiichi accidents,[2-3] as well as uranium accumulation near former mines and sites of nuclear fuel and weapons production.[4-5] Uranium contamination is also a concern in emerging energy-related cycles, such as the use of uraniferous black shales for hydrocarbon production[6] and the development of rare earth element ores for renewable energy production and storage.[7] Besides environmental issues, detailed knowledge of U chemistry is necessary for understanding uranium ore genesis[8] and for interpreting the U decay series and associated geochronometers.[9]

The behavior of U in the subsurface is controlled by its interactions with minerals, bacteria, and soluble groundwater constituents, yet limited mechanistic understanding of these reactions hinders broad efforts to predict and model U transformations and mobility. A particular knowledge gap is the behavior of U under reducing conditions that are naturally occurring or induced as part of remediation activities. Reduction of U^{6+} (the stable valence state in equilibrium with oxygenated water) to U^{4+} can result in a dramatic decrease of U solubility due to precipitation of the mineral uraninite, UO_{2+x}. Previous studies have shown that both bacteria and abiotic reductants can reduce U^{6+} to U^{4+}, resulting in uraninite formation.[10-13] Extensive research has consequently focused on characterization of the stability of uraninite phases.[14-16] However, recent spectroscopic evidence suggests that U^{4+} in sediments does not form uraninite on the time scale of months to years.[17-20] Laboratory studies indicate that phosphate or

41   phosphoryl groups complex U^{4+} and inhibit uraninite formation. [21-24] Phosphate-bound U^{4+} was

42   found subsequently to be more labile to dissolution or reoxidation than uraninite.[17,25]

43   Additionally, bacterial strain and physiology appear to have an effect on the nature of U^{4+}

44   produced during respiration on U^{6+}, most likely through control of the chemical conditions at the

45   location of electron transfer.[21] The identification of various U^{4+} species with stabilities different

46   from that of uraninite has profound implications for prediction of U transport, yet none of the

47   current field-scale models account for U^{4+} species other than a uraninite phase.[26-27] Indeed, there

48   is a pressing need to characterize the factors controlling the formation of non-uraninite U^{4+}

49   species, their molecular-scale structures, and their stability to solubilization and oxidation.

50   In contrast to (bio)mineralization of U^{4+}, the role of mineral surfaces in U^{4+} speciation

51   has been largely overlooked. Subsurface environments may not always contain high phosphate

52   or high biomass concentrations, but typically they have high mineral surface:U ratios. The

53   abundance of mineral surface sites in natural systems suggests a potentially significant role for

54   them in controlling U^{4+} speciation and stability. Although the low solubility of uraninite suggests

55   that it may be the thermodynamically stable U^{4+} state in many systems, the potential of high-

56   affinity mineral sites to complex U^{4+} atoms for significant periods of time and thus affect U

57   transport has not been examined. Previous investigations of U^{6+} reduction in phosphate-free

58   mineral suspensions have consistently observed the formation of nanoparticulate uraninite.[23, 28-32]

59   To date, only one study has identified complexed U^{4+} species on the surface of a mineral (Ti-

60   doped magnetite).[33]

61   Here we establish that model minerals can bind U^{4+} in inner-sphere surface complexes

62   that are stable with respect to uraninite formation over extended periods of time. We used

63   synchrotron x-ray spectroscopy and high-resolution transmission electron microscopy to

64   investigate the speciation of U^{4+} produced (a) in the presence of rutile (α-TiO$_2$) after reduction of

65   U^{6+} by the soluble electron shuttle AH$_2$QDS and (b) by the solid-phase reductant magnetite

66   (Fe$_3$O$_4$). In both cases, we observed the stabilization of adsorbed U^{4+} species at low U:surface

67   ratios that are more typical of environmental conditions. These findings provide a framework for

68   explaining the observations of non-uraninite U^{4+} in sediments and necessitate a paradigm shift in

69   the modeling of U transport, namely the inclusion of U^{4+} surface complexation reactions in

70   addition to uraninite and U^{4+}-biomineral formation. The findings also indicate a need for

71   extensive new research on U^{4+} speciation and stability to constrain appropriate reaction pathways

72   for reactive transport models.

73

74   **Experimental**

75   **Magnetite synthesis and characterization**

76   Details on the synthesis and characterization of the magnetite (Fe$_3$O$_4$) nanoparticles are

77   provided in the SI text and in previous work.[34] Briefly, a stirred solution of 0.2 M FeCl$_3$·6H$_2$O

78   and 0.1 M FeCl$_2$·4H$_2$O was titrated under anoxic conditions to a pH of ~9.5 with 10 M NaOH to

79   precipitate magnetite. Characterization showed only stoichiometric magnetite (Fe$_3$O$_4$, Fe^{2+}/Fe^{3+}

80   = 0.48 ± 0.02) with a particle size of 13.3 ± 5.7 nm (1 σ) and Brunauer-Emmett-Teller (BET)

81   surface area of 67.1 m^2/g. The magnetite suspensions were stored under anoxic conditions until

82   use.

83   **Rutile characterization**

84   The rutile form of TiO$_2$ (α-TiO$_2$) was purchased from Alfa-Aesar. Characterization by x-ray

85   diffraction confirmed the presence of only rutile. The particles size measured by scanning

86   electron microscopy (SEM) was 787 ± 479 nm, and the BET surface area was 4.1 m^2 g^{-1}.

87 **Reaction of U^{6+} with Fe$_3$O$_4$**

88   Fe$_3$O$_4$ suspensions of 5, 30, 60 and 120 g L^{-1} were prepared under strict anoxic conditions by

89 centrifuging the stock Fe$_3$O$_4$ suspension and resuspending the particles in 5 to 15 mL of 2 mM

90 NaHCO$_3$ buffer or 50 mM MOPS buffer, both prepared in deoxygenated deionized (DI) H$_2$O (18

91 MΩ·cm). Except for the centrifugation step, the Fe$_3$O$_4$ solids were not washed to prevent

92 significant changes in the Fe^{2+}/Fe^{3+} ratio in the solids.

93   The pH of the Fe$_3$O$_4$ reactors was adjusted to a value of 7.2, as needed, with 0.5 M HCl and

94 0.5 M NaOH. The reactions with U^{6+} were initiated by spiking with 0.5 mM uranyl acetate from

95 a 0.1 M stock dissolved in 0.1 M HCl. The solution pH was readjusted to 7.2 after addition of U.

96 Reactors were shaken periodically over the initial reaction time of 2 to 5 days. Samples for the x-

97 ray absorption measurements were collected by centrifugation after 2 to 5 days and again after 4

98 or 6 months of aging at room temperature in the anoxic chamber.

99 **Reaction of U^{6+} with TiO2 and AH$_2$QDS.**

100   Suspensions of 10, 30, and 60 g L^{-1} TiO$_2$ were prepared under strict anoxic conditions by

101 adding TiO$_2$ to 15 mL of deoxygenated 2 mM NaHCO$_3$ buffer or 50 mM MOPS buffer, followed

102 by a spike of 0.5 mM U^{6+}. The solution pH was adjusted to 7.2, and U^{6+} was allowed to sorb to

103 the solids for 2 h. U^{6+} reduction was initiated by adding 2 mM AH$_2$QDS from a 25 mM stock

104 (details in SI text). Reactors were shaken by hand, sealed, and covered with aluminum foil to

105 prevent light-induced redox reactions. Solid samples were collected for x-ray absorption

106 measurements after 3 to 5 days of initial reaction and then after 11.8 months.

107 **Transmission electron microscopy.**

108   Samples for TEM imaging were prepared by centrifuging subsamples of the Fe$_3$O$_4$ and TiO$_2$

109 suspensions and resuspending them in deoxygenated DI water. Drops of the new suspensions

110   were immediately placed on carbon-coated 400 mesh Cu grids with holey carbon supports and

111   dried under anoxic conditions. The samples were kept anoxic until mounting onto the TEM

112   sample holder and insertion into the column of the microscope (<1 min exposure to air). Images

113   were acquired at 200 kV with a FEI CM30T TEM and an FEI Tecnai F20ST scanning TEM.

114   Further details can be found in the SI text.

115   **X-ray absorption spectroscopy.**

116   U L_{III} edge (17,166 eV) x-ray absorption spectroscopy was done at the MR-CAT/EnviroCAT

117   insertion device beamline (Sector 10-ID, Advanced Photon Source). The beamline utilizes a

118   LN_2-cooled Si (111) double-crystal monochromator and a Rh harmonic rejection mirror.

119   Fluorescence-mode spectra were collected using an Ar-filled ionization chamber. Samples were

120   kept at -100 °C to prevent photochemical reactions. Sample preparation and analysis procedures

121   are described in detail in the SI text.

122

123   **Results and Discussion**

124   The conditions and samples are summarized in Table 1. In the first series of experiments,

125   we chose TiO_2 as a redox-inactive substrate and reduced U^{6+} with the soluble reductant 9,10-

126   anthradihydroquinone-2,6-disulfonate (AH_2QDS). The AH_2QDS molecule is widely used as a

127   two-electron transfer mediator to simulate the electron shuttle compounds used by

128   microorganisms (oxidized form, AQDS, $E^0_{pH=7}$ = -0.184 V).[35] Ti^{4+} sites are relevant to U

129   speciation in many soils, sediments, and rocks where Ti is typically found in higher

130   concentrations (e.g., ~0.2 % by mass in soils) than known uranophile elements such as P (~0.06

131   %).[36] U^{6+} was adsorbed to TiO_2 in suspensions varying from 10 to 60 g L^{-1} (average surface

132   density of 7.5 to 1.3 U nm^{-2}; Table 1), and AH_2QDS was added subsequently. In the second

133 series of experiments, magnetite (Fe_3O_4) was used as both the reductant and the source of

134 binding sites for U. Fe_3O_4 is a common iron oxide found in geological materials, produced by

135 iron metal corrosion or through microbial respiration of Fe oxy-hydroxide minerals. [23, 28] Fe_3O_4

136 conducts and stores electrons in its structure and exchanges them with redox-active solution

137 components (including U^{6+}) via interfacial electron transfer reactions.[28, 30, 33-34, 37-38] We studied

138 the reaction of U^{6+} with Fe_3O_4 in suspensions of 5 to 120 g L^{-1} (U surface density of 0.9 to 0.04

139 U nm^{-2}). We also varied the reaction time (from 2 days to 12 months) and the presence/absence

140 of bicarbonate (a strong complexant for U). In all reactors, >99% of the added U^{6+} was removed

141 from solution after <2 days.

142 **Table 1.** Experimental conditions and sample list

| Solids Concentration	Buffer	Surface area loading, m^2 L^{-1}	Surface uranium coverage, U nm^{-2}	Reaction time, day (months)[a]
TiO_2 (rutile)				
10 g L^{-1}	2 mM HCO_3^-	40	7.5	3.2
30 g L^{-1}	2 mM HCO_3^-	120	2.5	4.2
60 g L^{-1}	2 mM HCO_3^-	240	1.3	3.7
TiO_2 (rutile)				
10 g L^{-1}	50 mM MOPS	40	7.5	2.8
30 g L^{-1}	50 mM MOPS	120	2.5	3.7
60 g L^{-1}	50 mM MOPS	240	1.3	2.9
TiO_2 (rutile) – Long Term				
30 g L^{-1}	2 mM HCO_3^-	120	2.5	358 (11.8)
60 g L^{-1}	2 mM HCO_3^-	240	1.3	358 (11.8)
Magnetite				
5 g L^{-1}	2 mM HCO_3^-	300	0.9	1.6
30 g L^{-1}	2 mM HCO_3^-	1800	0.2	1.7
60 g L^{-1}	2 mM HCO_3^-	3600	0.08	1.7
120 g L^{-1}	2 mM HCO_3^-	7200	0.04	5.0
Magnetite				
5 g L^{-1}	50 mM MOPS	300	0.9	4.7
30 g L^{-1}	50 mM MOPS	1800	0.2	4.8
60 g L^{-1}	50 mM MOPS	3600	0.08	2.1
120 g L^{-1}	50 mM MOPS	7200	0.04	3.3
Magnetite – Long Term				
30 g L^{-1}	2 mM HCO_3^-	1800	0.2	190 (6.3)
60 g L^{-1}	2 mM HCO_3^-	3600	0.08	190 (6.3)
120 g L^{-1}	2 mM HCO_3^-	7200	0.04	116 (3.8)

143 [a] Reaction time in months in parentheses is calculated by using an average of 30.44
144 days/month

145

146   Electron transfer to U^{6+} was verified by x-ray absorption near-edge spectroscopy (XANES) at

147   the U L_{III}-edge (17,166 eV). Complete reduction to U^{4+} (>95% of solid-phase U) occurred under

148   the experimental conditions in all Fe_3O_4 and TiO_2/AH_2QDS systems (Fig. S1). A control reactor

149   with U^{6+} and TiO_2 but no added AH_2QDS did not produce U^{4+} (Fig. S1). These results are

150   consistent with previous studies where U^{6+} was reduced to U^{4+} by Fe_3O_4 or AH_2QDS, resulting

151   in uraninite formation.[21, 23, 28, 30, 32] However, the average speciation of U^{4+} in our systems

152   exhibited an unexpected dependence on U:surface ratio, as discussed below.

Effect of TiO_2 surface area on U^{4+} speciation

154   We characterized the molecular structure around U^{4+} by using extended x-ray absorption fine-

155   structure (EXAFS) spectroscopy (experimental details in SI text). Trends in the Fourier-

156   transformed EXAFS data with changing TiO_2 mineral loading are illustrated in Figs. 1A and

157   S2A.
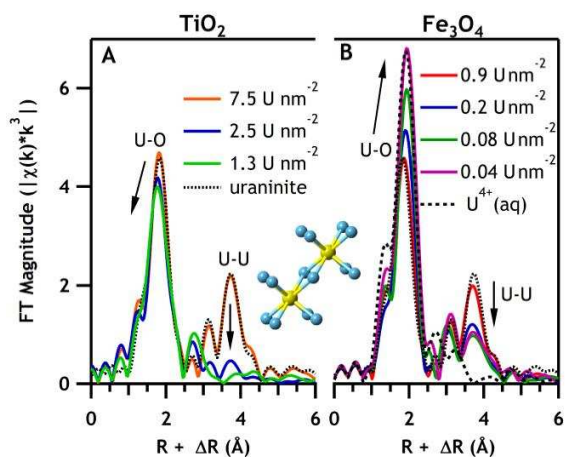
Fig. 1. Fourier transform (FT) of the U L_{III}-edge EXAFS data from U^{4+} produced by reactions of

160   U^{6+} with (A) TiO_2 and 2 mM AH_2QDS and (B) Fe_3O_4 as a solid-phase reductant. Data are from

161   reactors with 2-mM $NaHCO_3$ at pH 7.2. Lines in color show the data from samples at different U

162   surface densities. Standards are nanoparticulate uraninite and an aqueous solution of U^{4+} in 0.5

163   M H_2SO_4 (dotted and dashed lines, respectively). Arrows show trends with decreasing U density

164   (increasing surface area). The molecular model illustrates the U-U coordination in uraninite. FTs

165   are done over k = 2.2-10.4 Å^{-1} with a Hanning window sill 1 Å^{-1} wide.

166

167   The salient feature is the doublet peak corresponding to the dioxo-bridging bonds between the

168   U^{4+} atoms in uraninite (labeled U-U). The presence and amplitude of the U-U peak indicate that

169   the predominant form of U^{4+} at the high average surface density of 7.5 U nm^{-2} is nanoparticulate

170   uraninite, whereas the lack of amplitude at 1.3 U nm^{-2} indicates the predominance of adsorbed

171   non-uraninite U^{4+} species. The spectral features of the adsorbed U^{4+} species are different from

172   those of non–uraninite U^{4+} observed in bacterial systems and in sediments,[17-19, 21-24, 39-40]

173   indicating the sensitivity of EXAFS to this distinct form of U^{4+}. The molecular structure derived

174   from fits of the data indicates inner-sphere complexation between U^{4+} and Ti^{4+} centers (details in

175   SI text; Fig. S3). Adsorption geometries on the surface of TiO_2 that are consistent with the

176   EXAFS data are illustrated in Fig. 2A.

177

178
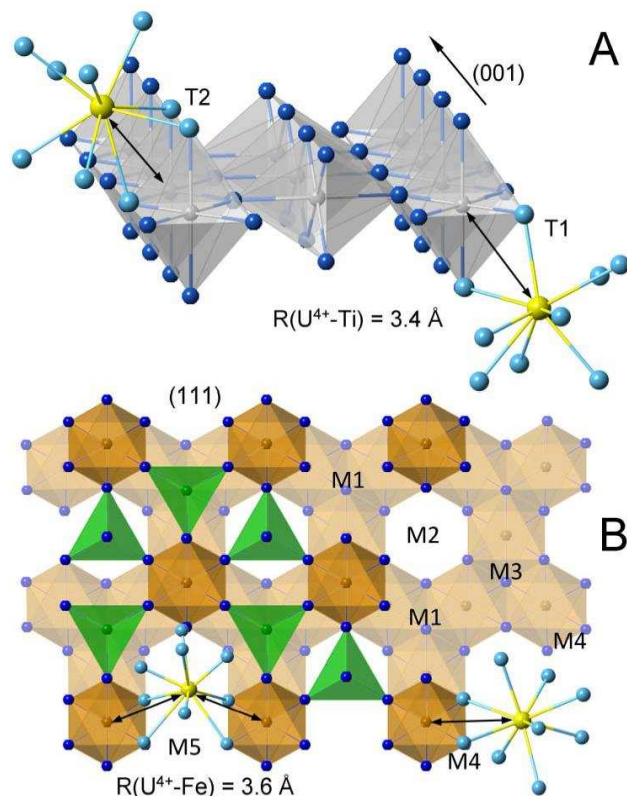
Fig. 2. Molecular models of U^{4+} adsorption. (A) U^{4+}-TiO_2 complexes. The fragment shows the

edge-sharing Ti-O_6 octahedra (gray) in rutile. T1 depicts adsorption of U^{4+} (yellow) to the edge

of a terminal Ti octahedron. T2 depicts adsorption of U^{4+} to the corners or the free edges of two

edge-sharing Ti octahedra. (B) U^{4+}-Fe_3O_4 complexes. The fragment shows the (111) surface of

Fe_3O_4, with some Fe centers removed to illustrate possible adsorption sites. Fe octahedra are in

orange; Fe tetrahedra are in green. The light-orange Fe octahedra are situated in the layer below

the dark-orange octahedra. The symmetric sites M1-M3 were found to be inconsistent with the

distances obtained in the EXAFS fits. The likely sites for U^{4+} adsorption (M4 and M5) are

shown.

188

The findings from the EXAFS analysis are corroborated by transmission electron microscopy

190 (TEM). Fig. 3A reveals the formation of particles sized 2-4 nm in samples with U:surface

191 density of 7.5 U nm^{-2}. The particles have lattice fringe spacing of 0.32 nm (Fig. S4), consistent

192 with the (111) lattice spacing in uraninite (0.316 nm).[41] Selected-area electron diffraction

193 (SAED) patterns are also consistent with those of uraninite (Fig. S4). In contrast to the 7.5 U nm^{-2}

194 sample, uraninite particles are absent at the lower 1.3 U nm^{-2} coverage (Fig. 3B). Taken

195 together, our EXAFS and TEM results suggest that U^{4+} is stabilized as an adsorbed species when

196 the TiO_2 surface loading is high enough to provide a sufficient number of high-affinity binding

197 sites.
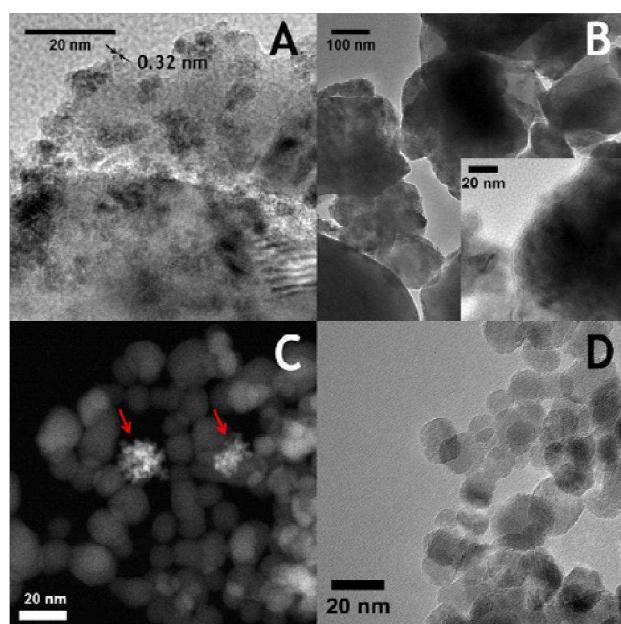
198

199 **Fig. 3.** Transmission electron microscopy images from the TiO_2/AH_2QDS and Fe_3O_4 reactors

200 with U^{6+} at high and low U surface density. (A) A bright-field image of a TiO_2 suspension with

201 7.5 U nm^{-2} showing 2- to 4-nm particles with lattice fringe spacing of 0.32-nm, which are more

202 clearly displayed in Fig. S4. (B and inset) Bright-field images of TiO_2 particles containing 1.3 U

203 nm^{-2}. No UO_2 nanoparticles are observed. (C) High-angle annular dark-field (HAADF) STEM,

204 showing Z-contrast between Fe_3O_4 and brighter uraninite (red arrows) nanoparticles (0.9 U nm^{-}

205   ^{2}). (D) Representative bright-field image of 0.04 U nm^{-2} sample, indicating the absence of

206   uraninite nanoparticles. Additional TEM images are included in the SI.

207

208   **Effect of Fe$_3$O$_4$ surface area on U^{4+} speciation**

209   The trends in the U^{4+} EXAFS spectra with changing U:Fe$_3$O$_4$ surface loading are

210   illustrated in Figs. 1B and S2B. At the highest average density of 0.9 U nm^{-2}, the EXAFS

211   spectrum is identical to that of the uraninite standard (Fig. 1B). Formation of UO$_2$ during U^{6+}

212   reduction by Fe$_3$O$_4$ has been observed consistently in previous studies carried out at similarly

213   high U:surface ratios.[23, 28, 30, 32] Upon decreasing the average U surface coverage to 0.2, 0.08, and

214   0.04 U nm^{-2} we observe significantly smaller amplitudes of the U-U doublet (Fig. 1B and S2B).

215   This trend is accompanied by an increase in the amplitude and distance of the peak

216   corresponding to O coordination (R + $\Delta \sim$ 1.8 Å; Fig. 1B). Consistent and significant changes

217   with U surface density can also be observed in the k$^3\chi$(k) data (Fig. S5B). Fits of the data from

218   the sample at the lowest coverage (0.04 U nm^{-2}) indicate a larger O coordination number (10 vs.

219   8) and a larger U^{4+}-O distance (2.43 vs. 2.35 Å) relative to uraninite (SI text; Figs. S5, S6; Table

220   S1). Coordination numbers of 9-10 and longer U^{4+}-O bonds of 2.41-2.45 Å have been

221   determined previously for non-uraninite U^{4+} species in solution and in solids.[42-43] The longer U-

222   O bonds observed here at 0.04 U nm^{-2} coverage suggest a predominantly non-uraninite U^{4+}

223   speciation. Shell-by-shell fits of the features up to R + Δ = 4.2 Å produced a best fit with 10 O

224   atoms around U^{4+} at 2.43 Å, ~1.5 Fe atoms at 3.59 Å, and ~5 O atoms at 4.30 Å (Table S1).

225   Models with a U shell at R ~3.9 Å resulted in lower-quality fits and inconsistent reproduction of

226   the data at different k-weights of the Fourier transform (SI text; Figure S6).

227   Despite the presence of a peak where the U shell contributes in uraninite (Fig. 1B), the

228   analysis above indicates that this peak is not due to U-U coordination in uraninite for samples

229   with low U coverage. The peak from the Fe shell and its distance from U^{4+} suggest inner-sphere,

230   bidentate complexation of U^{4+} to =FeO sites. Possible edge-sharing complexes at the (111)

231   surface of Fe_3O_4 are illustrated in Fig. 2B. The low surface coverage at which these U^{4+}

232   complexes are predominant (0.04 U nm^{-2}) suggests that these mononuclear U^{4+} species are

233   formed at defect sites or at lattice step/kink sites on the Fe_3O_4 surface, possibly in chelate-type

234   complexes (e.g., M5 in Fig. 2B).

235   TEM corroborates the presence of UO_2 nanoparticles at 0.9 U nm^{-2} average surface

236   density (Fig. 3C). Images collected in high-angle annular dark-field mode emphasize high-Z

237   elements in the sample and indicate that the sub-10 nm particles of uraninite form clusters with

238   other uraninite particles. Our observation of uraninite clusters detached from the iron oxide is

239   unusual. Previous studies observed association of individual uraninite particles with the edges of

240   green rust[31] or with large crystals of Fe_3O_4.[30] Reasons for the segregation of uraninite may relate

241   to the mechanisms of reduction, which we discuss further down, together with other findings. In

242   contrast to the samples at high U:surface ratio, extensive TEM imaging of the 0.04 U nm^{-2}

243   sample revealed no evidence for U-rich particles (Fig. 3D), supporting the conclusion of

244   adsorbed U^{4+} from the EXAFS analysis.

245   **Effect of bicarbonate on U^{4+} speciation**

246   Our experimental design included parallel systems with and without bicarbonate to test

247   for its effects on redox reactivity or on U^{4+} speciation. An additional consideration was to test

248   whether carbonate associated with the adsorbed U^{4+} atoms and was thus responsible for the

249   stabilization of the non-uraninite U^{4+} species. Carbonate has been shown to complex U^{4+}, but at

250 significantly higher carbonate:U ratios than we used.[42] Fig. S7 compares spectra between our

251 systems with and without bicarbonate for different U surface densities on TiO_2. The presence of

252 2 mM bicarbonate has little or no effect on the EXAFS spectrum of the reduced U^{4+} species. At

253 the U:mineral loading of 7.5 U nm^{-2} in the TiO_2 system, the features corresponding to uraninite

254 appear slightly more pronounced in the absence of bicarbonate and indicate a slightly more

255 abundant or a slightly more ordered uraninite phase in that sample. For the lower surface

256 coverages of 2.5 and 1.3 U nm^{-2} the spectra with or without bicarbonate are identical.

257   As for the TiO_2 system above, the absence of bicarbonate in the Fe_3O_4 reactors results in

258 slightly larger amplitude of the U-U features relative to the corresponding systems with added

259 bicarbonate (Fig. S7). Although these spectral trends appear consistently for loadings of 0.9, 0.2,

260 and 0.08 U nm^{-2}, numerical analysis of the data could not establish a statistically significant

261 increase in the average O or U coordination numbers, suggesting that bicarbonate does not have

262 a significant effect on the average U^{4+} speciation at the surface (i.e., <10% of total U may be

263 affected).

264   The results indicate that carbonate does not affect the adsorption mechanism of U^{4+} to

265 TiO_2 or Fe_3O_4 surfaces and that carbonate is not the reason for the stabilization of non-uraninite

266 U^{4+}. Indeed, both shell-by-shell modeling of the EXAFS and the independence of the spectra on

267 bicarbonate suggest that the non-uraninite U^{4+} species are stabilized by inner-sphere

268 complexation to binding sites on the TiO_2 or Fe_3O_4 surfaces.

269 **Stability of adsorbed U^{4+} over time**

270   We investigated the stability of surface-complexed U^{4+} species under anoxic conditions

271 by characterizing a subsample of the reactors after ~3 days of reaction and then after several

272 months (Table 1). Only the sample series with 2 mM bicarbonate was examined. The EXAFS

273   data from the TiO_2 reactors with 3.5 and 1.2 U nm^{-2} (low U coverage) (Fig. 4A) show identical

274   spectra after 3 days and after 11.8 months of reaction, suggesting that the TiO_2-complexed U^{4+}

275   species are not transformed to uraninite over at least a year, even with a minor uraninite

276   component present in the 3.5 U nm^{-2} sample to provide nucleation sites. Notably, the non-

277   uraninite U^{4+} species are stable in the presence of bicarbonate, which presumably accelerates

278   solubilization of monomeric U^{4+} and facilitates migration between sites on the TiO_2 surface and

279   the sites of uraninite nucleation.[25]

280
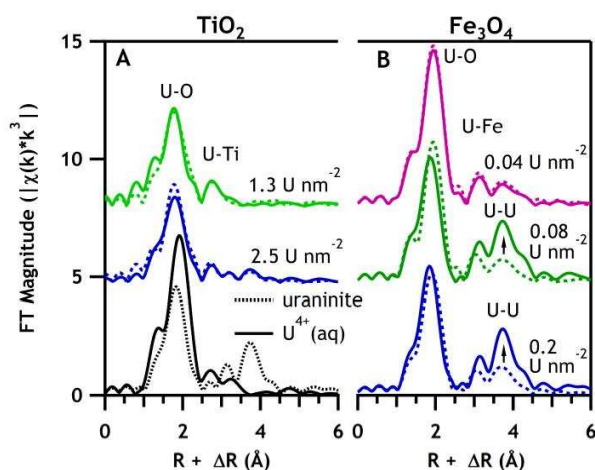
282   **Fig. 4.** U L_{III}-edge EXAFS showing the effect of aging on the U^{4+} speciation in (A) TiO_2

283   suspensions and (B) Fe_3O_4 suspensions. TiO_2 suspensions were allowed to react for 3 days

284   (dotted line) and 11.8 months (solid line). Fe_3O_4 suspensions were aged for 2-5 days (dotted

285   lines) and 6 months (solid lines, 0.2 U nm^{-2} and 0.08 U nm^{-2}) or 4 months (solid line, 0.04 U nm^{-2})

286   in 2-mM $NaHCO_3$ solution, pH 7.2. U^{4+} standards are shown in the lower portion of panel A

287   for comparison. Arrows indicate the growth of the U-U peak with time in the magnetite samples

288   with higher U coverage.

289

290   To test whether formation of uraninite in the TiO_2 system was kinetically or

291   thermodynamically inhibited, we reacted pre-formed uraninite with TiO_2 at the same U^{4+}:mineral

292   ratios as in the 1.2 U nm^{-2} sample (details in SI text). We did not observe evolution of the

293   starting uraninite to U^{4+} adsorbed to TiO_2 after 1 month at 70 °C (Fig. S8). The question of

294   kinetic or thermodynamic limitation therefore remains open. Regardless of whether uraninite or

295   the TiO_2-adsorbed U^{4+} species is thermodynamically more stable, progress towards equilibrium

296   appears to be slow.

297   The U^{4+} species in the Fe_3O_4 system exhibit different stabilities relative to the TiO_2 system

298   (Fig. 4B). The non-uraninite U^{4+} species in the 0.04 U nm^{-2} system (low U coverage) remained

299   unaltered after 4 months, indicating significant stabilization of adsorbed U^{4+} at high-affinity

300   binding sites on the Fe_3O_4 surface. In contrast, the predominantly non-uraninite U^{4+} speciation in

301   the 0.08 and 0.2 U nm^{-2} system shifted toward nanoparticulate uraninite after 6 months of

302   reaction time, suggesting that the U^{4+} species on the Fe_3O_4 surface are less stable than non-

303   uraninite U^{4+} stabilized on the TiO_2 surface. The growth of uraninite in the Fe_3O_4 system may be

304   due to a weaker bond between the U^{4+} atoms and the Fe_3O_4 surface relative to the surface of

305   TiO_2. An alternative explanation may be the known role of Fe_3O_4 as a reservoir for electrons,[28,]

306   [34, 37] which would allow for temporary oxidation of U^{4+} to U^{5+} or U^{6+}. The consequent increase in

307   U mobility and transport to a U^{6+} reduction site that is closer to a uraninite nucleation site could

308   promote uraninite growth over time (Fig. 5).

309
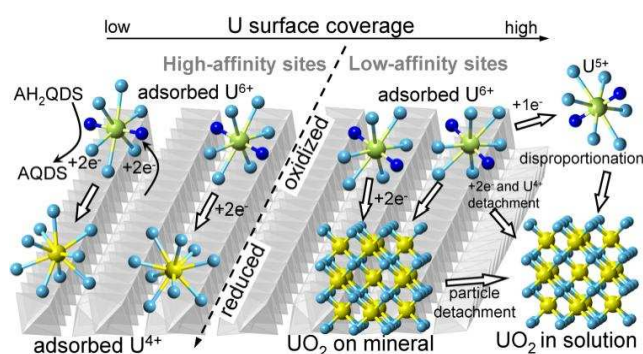
310

311 **Fig. 5.** Conceptual model for U^{6+} reduction at TiO_2 and Fe_3O_4 surfaces. The soluble shuttle (for

312 TiO_2) and interfacial electron transfer (for Fe_3O_4) pathways are illustrated with the U^{6+} atom to

313 the top left. The initially adsorbed U^{6+} atoms are depicted at the top, the reduced U^{4+} species at

314 the bottom. At low surface coverage, reduced U^{4+} atoms are stabilized individually at the high-

315 affinity sites (left). At high surface coverage, the more labile U^{4+} atoms at the low-affinity sites

316 combine to form uraninite (right). A possible U^{5+} disproportionation pathway is also illustrated.

317 The axial O atoms of U^{6+} or U^{5+} are emphasized in dark blue.

318

319 **Uranium dynamics at the mineral surface**

320   Uranium is known to undergo two single-electron transfer steps during reduction: UO_2^{2+} to

321 UO_2^+ and UO_2^+ to U^{4+}.[44] Depending on solution conditions, two UO_2^+ (U^{5+}) molecules can

322 undergo a disproportionation reaction, producing U^{4+} and UO_2^{2+}.[45] Ample evidence exists to

323 suggest that U^{5+} disproportionation reactions are kinetically hindered at the surface of Fe-bearing

324 minerals.[9, 37-38, 46] However, reports are conflicting as to whether the formation of U^{4+} involves

325 (a) disproportionation of U^{5+} at the surface[9] or (b) two subsequent electron transfers from Fe^{2+}

326 (shown conceptually in Fig. 5).[37, 47] In either case, the processes operative in our systems must be

327 consistent with the observed valence state, localization, and speciation of U, as well as the

328 observed aging of U^{4+} surface complexes to uraninite.

329   While it is tempting to conclude that the segregated nanoclusters of uraninite (Fig. 3C)

330   observed in the Fe_3O_4 sample with 0.9 U nm^{-2} result directly from U^{5+} disproportionation

331   reactions (Fig. 5, right side), our observation of U^{4+}-Fe surface complexes aging to uraninite

332   suggest that precipitation of uraninite may be due to solubilization of adsorbed U^{4+} in the Fe_3O_4

333   samples with 0.2 and 0.08 U nm^{-2}. Alternatively, formation of uraninite nanoparticles from

334   adsorbed U^{4+} may also be explained through a dynamic redox equilibrium between U^{4+}/U^{5+} and

335   Fe^{2+}/Fe^{3+}, whereby the electron exchange between Fe^{3+} and U^{4+} controls the solution activity of

336   U^{5+} and hence the formation of uraninite via the disproportionation pathway (Fig. 5). Another

337   possible mechanism for uraninite formation may be Ostwald ripening on the surface of Fe_3O_4,

338   with subsequent detachment and agglomeration of the uraninite particles. Regardless of the

339   pathway for uraninite formation, our results suggest that the process begins with single U^{4+}

340   atoms complexed at the Fe_3O_4 surface and that the predominant U^{4+} speciation is controlled by

341   the availability of high-affinity surface sites.

342   Significant stabilization of adsorbed U^{4+} is observed when TiO_2 is present as the mineral

343   substrate. Soluble AH_2QDS has been shown to reduce U^{6+} in solution, leading to nanoparticulate

344   uraninite.[21] This result, together with the lack of reaction between TiO_2 and pre-formed UO_2 in

345   our aging experiments, suggests that TiO_2-sorbed U^{4+} is not formed after reduction of aqueous

346   U^{6+} species. Instead, electron transfer likely occurs between AH_2QDS and adsorbed U^{6+} species

347   (left side, Fig. 5). Studies of U^{6+} adsorption to TiO_2 have shown that U^{6+} forms primarily inner-

348   sphere complexes at low U coverage (<~1 U nm^{-2}) and outer-sphere complexes at higher U

349   coverage.[48] The correlation with the dependence of U^{4+} speciation on U surface coverage

350   determined in our study (adsorbed U^{4+} at 1.3 U nm^{-2} and nanoparticulate uraninite at 7.5 U nm^{-2})

351   suggests that reduction of outer-sphere-sorbed U^{6+} results in uraninite, whereas reduction of

352   inner-sphere-sorbed U^{6+} results in surface-complexed U^{4+}. The lack of aging of the U^{4+}-Ti

353   complexes indicates that sorption to high-affinity Ti sites (left side, Fig. 5) provides significant

354   stabilization of U^{4+} against desorption or Ostwald ripening and subsequent uraninite formation.

355

356   **Environmental implications**

357   This study significantly expands the diversity of U^{4+} species that may control the transport of

358   U in environmental systems and underscores the need for improved description of U^{4+}

359   speciation. Although several studies have now observed non-uraninite U^{4+} species in sediments

360   and soils,[18-20, 49] the molecular structure and the mechanisms leading to these U^{4+} species remain

361   uncertain. Transformations in sediments are governed by highly coupled biotic-abiotic

362   interactions, and the pathway through which an observed U^{4+} species is produced can be difficult

363   to ascertain. Our study demonstrates that =TiO and =FeO sites can stabilize non-uraninite,

364   surface-adsorbed U^{4+} species, which are distinct chemically and spectroscopically from the

365   carbonate- or phosphate-bound U^{4+} complexes observed during enzymatic reduction of U^{6+}.[21-22,

366   24, 50] It is likely that many other subsurface minerals have high-affinity sites (e.g., at steps or

367   kinks on their surface) that can stabilize adsorbed U^{4+} at sufficiently low U coverage. Our results

368   also suggest that U^{4+} can be stabilized on mineral surfaces both as a result of abiotic reduction by

369   Fe^{2+} (e.g., U^{6+} reduction by Fe_3O_4) and in coupled biotic-abiotic reduction pathways involving an

370   electron shuttle (e.g., U^{6+} reduction by AH_2QDS in the presence of TiO_2). These observations

371   provide a basis for establishing a connection (or lack thereof) between observed U^{4+} speciation

372   and reduction pathways of U^{6+} in future studies.

373   The discovery of an array of non-uraninite U^{4+} species here and in previous studies[18, 20-22,

374   24, 49-50] points to significant gaps in our understanding of U^{4+} biogeochemistry. Such gaps have

375   immediate bearing on the ability of geochemical models to predict the behavior of U over the

376   short and long term. If U^{4+} surface-complexes are less stable than uraninite, then the common

377   assumption of reductive precipitation of U^{4+} as uraninite will under-predict the mobility of U in

378   groundwaters and vice versa. The lack of thermodynamic parameters (e.g., ΔG_f^0 or $E^{0'}$) for the

379   formation of U^{4+}-mineral complexes hinders modeling efforts focused on determining U stability

380   with redox conditions, and additional complications arise for modeling the kinetics of these

381   reactions. While our study suggests that U^{4+}-Fe complexes are a relatively stable but likely a

382   transitory phase in the formation of uraninite, the lack of U^{4+}-Ti complex transformations over

383   nearly a year indicates that U^{4+}-Ti complexes may be important in U dynamics over time scales

384   relevant to the remediation of contaminated sediments. U^{4+} complexes to =TiO sites may be

385   precursors to the naturally-occurring mineral brannerite ($U^{4+}Ti_2O_6$) and help explain its

386   formation. Also lacking is information on the stability of U^{4+} surface complexes to oxidation by

387   common groundwater oxidants such as dissolved O_2 and nitrite (NO_2^-). Uraninite and U^{4+}

388   complexes to =FeO sites are likely to be less susceptible to oxidation when in contact with

389   Fe_3O_4, given that Fe_3O_4 is capable of U^{6+} reduction even when its Fe^{2+}/Fe^{3+} ratio is significantly

390   more oxidized than the stoichiometric 0.5.[28, 51]

391   The strong complexation between U^{4+} and =TiO sites may be useful for technological

392   applications related to water purification. The TiO_2 surface appears to have high density of sites

393   for U^{4+} complexation (~1 U nm^{-2}). If reduction of U^{6+} to U^{4+} leads to lower aqueous U

394   concentrations regardless of the speciation of U^{4+}, sequestering U as adsorbed U^{4+} species rather

395   than nanoparticulate uraninite might be advantageous. Strong adsorption of U^{4+} to large TiO_2-

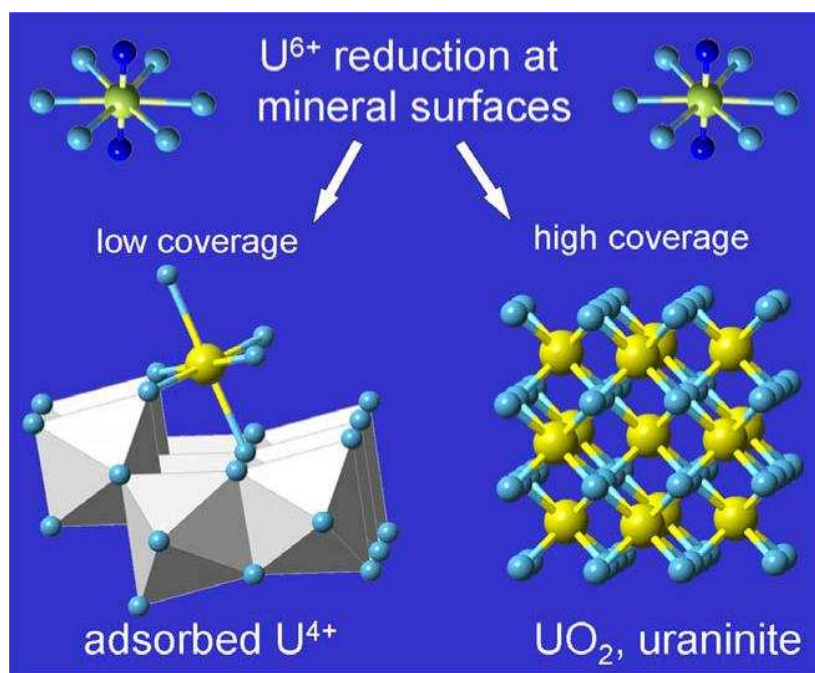396   coated particles can lower the risk of colloidal U transport.

397

398   **Acknowledgements**

408   **Supporting Information**. More details on the experimental methods, TEM imaging, and

409   EXAFS data analysis are included in Supporting Information. This material is available free of

410   charge via the Internet at http://pubs.acs.org.

411

412   **Table of Contents (TOC) Art**

413

References

(1)   Macfarlane, A., It's 2050: Do you know where your nuclear waste is? Bull. Atom. Sci. **2011,** 67 (4), 30-36.

(2)   Cuddihy, R. G.; Finch, G. L.; Newton, G. J.; Hahn, F. F.; Mewhinney, J. A.; Rothenberg, S. J.; Powers, D. A., Characteristics of radioactive particles released from the Chernobyl nuclear reactor. Environ. Sci. Technol. **1989,** 23 (1), 89-95.

(3)   Burns, P. C.; Ewing, R. C.; Navrotsky, A., Nuclear Fuel in a Reactor Accident. Science **2012,** 335 (6073), 1184-1188.

(4)   Ahearne, J. F., Radioactive waste: The size of the problem. Phys. Today **1997,** 50 (6), 24-29.

(5)   Gavrilescu, M.; Pavel, L. V.; Cretescu, I., Characterization and remediation of soils contaminated with uranium. J. Hazard. Mater. **2009,** 163 (2-3), 475-510.

(6)   Barbot, E.; Vidic, N. S.; Gregory, K. B.; Vidic, R. D., Spatial and Temporal Correlation of Water Quality Parameters of Produced Waters from Devonian-Age Shale following Hydraulic Fracturing. Environ. Sci. Technol. **2013,** 47 (6), 2562-2569.

(7)   Long, K. R.; Gosen, B. S.; Foley, N. K.; Cordier, D. The principal rare earth elements deposits of the United States: A summary of domestic deposits and a global perspective; 2010.

(8)   Richard, A.; Rozsypal, C.; Mercadier, J.; Banks, D. A.; Cuney, M.; Boiron, M.-C.; Cathelineau, M., Giant uranium deposits formed from exceptionally uranium-rich acidic brines. Nat. Geosci. **2012,** 5 (2), 142-146.

(9)   Renock, D.; Mueller, M.; Yuan, K.; Ewing, R. C.; Becker, U., The energetics and kinetics of uranyl reduction on pyrite, hematite, and magnetite surfaces: A powder microelectrode study. Geochim. Cosmochim. Acta **2013,** 118 (0), 56-71.

(10)   Wall, J. D.; Krumholz, L. R., Uranium Reduction. Annu. Rev. Microbiol. **2006,** 60 (1), 149-166.

(11)   Suzuki, Y.; Kelly, S. D.; Kemner, K. M.; Banfield, J. F., Radionuclide contamination - Nanometre-size products of uranium bioreduction. Nature **2002,** 419 (6903), 134-134.

(12)   Lovley, D. R.; Phillips, E. J. P.; Gorby, Y. A.; Landa, E. R., Microbial reduction of uranium. Nature **1991,** 350 (6317), 413-416.

(13)   O'Loughlin, E. J.; Boyanov, M. I.; Antonopoulos, D. A.; Kemner, K. M., Redox Processes Affecting the Speciation of Technetium, Uranium, Neptunium, and Plutonium in Aquatic and Terrestrial Environments. American Chemical Society: 2011; Vol. 1071, p 477-517.

(14)   Campbell, K. M.; Veeramani, H.; Ulrich, K.-U.; Blue, L. Y.; Giammar, D. E.; Bernier-Latmani, R.; Stubbs, J. E.; Suvorova, E.; Yabusaki, S.; Lezama-Pacheco, J. S.; Mehta, A.; Long,

449   P. E.; Bargar, J. R., Oxidative Dissolution of Biogenic Uraninite in Groundwater at Old Rifle,
450   CO. Environ. Sci. Technol. **2011,** 45 (20), 8748-8754.

451   (15)   Ulrich, K.-U.; Ilton, E. S.; Veeramani, H.; Sharp, J. O.; Bernier-Latmani, R.; Schofield,
452   E. J.; Bargar, J. R.; Giammar, D. E., Comparative dissolution kinetics of biogenic and
453   chemogenic uraninite under oxidizing conditions in the presence of carbonate. Geochim.
454   Cosmochim. Acta **2009,** 73 (20), 6065-6083.

455   (16)   Ulrich, K. U.; Singh, A.; Schofield, E. J.; Bargar, J. R.; Veeramani, H.; Sharp, J. O.;
456   Bernier-Latmani, R.; Giammar, D. E., Dissolution of biogenic and synthetic UO_2 under varied
457   reducing conditions. Environ. Sci. Technol. **2008,** 42 (15), 5600-5606.

458   (17)   Sharp, J. O.; Lezama-Pacheco, J. S.; Schofield, E. J.; Junier, P.; Ulrich, K. U.; Chinni, S.;
459   Veeramani, H.; Margot-Roquier, C.; Webb, S. M.; Tebo, B. M.; Giammar, D. E.; Bargar, J. R.;
460   Bernier-Latmani, R., Uranium speciation and stability after reductive immobilization in aquifer
461   sediments. Geochim. Cosmochim. Acta **2011,** 75 (21), 6497-6510.

462   (18)   Kelly, S. D.; Wu, W.-M.; Yang, F.; Criddle, C. S.; Marsh, T. L.; O'Loughlin, E. J.;
463   Ravel, B.; Watson, D.; Jardine, P. M.; Kemner, K. M., Uranium transformations in static
464   microcosms. Environ. Sci. Technol. **2010,** 44 (1), 236-242.

465   (19)   Kelly, S. D.; Kemner, K. M.; Carley, J.; Criddle, C.; Jardine, P. M.; Marsh, T. L.;
466   Phillips, D.; Watson, D.; Wu, W. M., Speciation of uranium in sediments before and after in situ
467   biostimulation. Environ. Sci. Technol. **2008,** 42 (5), 1558-1564.

468   (20)   Bargar, J. R.; Williams, K. H.; Campbell, K. M.; Long, P. E.; Stubbs, J. E.; Suvorova, E.
469   I.; Lezama-Pacheco, J. S.; Alessi, D. S.; Stylo, M.; Webb, S. M.; Davis, J. A.; Giammar, D. E.;
470   Blue, L. Y.; Bernier-Latmani, R., Uranium redox transition pathways in acetate-amended
471   sediments. Proc. Natl. Acad. Sci. USA **2013,** 110 (12), 4506-4511.

472   (21)   Boyanov, M. I.; Fletcher, K. E.; Kwon, M. J.; Rui, X.; O'Loughlin, E. J.; Löffler, F. E.;
473   Kemner, K. M., Solution and microbial controls on the formation of reduced U(IV) species.
474   Environ. Sci. Technol. **2011,** 45 (19), 8336-8344.

475   (22)   Fletcher, K. E.; Boyanov, M. I.; Thomas, S. H.; Wu, Q. Z.; Kemner, K. M.; Loffler, F. E.,
476   U(VI) reduction to mononuclear U(IV) by Desulfitobacterium species. Environ. Sci. Technol.
477   **2010,** 44 (12), 4705-4709.

478   (23)   Veeramani, H.; Alessi, D. S.; Suvorova, E. I.; Lezama-Pacheco, J. S.; Stubbs, J. E.;
479   Sharp, J. O.; Dippon, U.; Kappler, A.; Bargar, J. R.; Bernier-Latmani, R., Products of abiotic
480   U(VI) reduction by biogenic magnetite and vivianite. Geochim. Cosmochim. Acta **2011,** 75 (9),
481   2512-2528.

482   (24)   Bernier-Latmani, R.; Veeramani, H.; Vecchia, E. D.; Junier, P.; Lezama-Pacheco, J. S.;
483   Suvorova, E. I.; Sharp, J. O.; Wigginton, N. S.; Bargar, J. R., Non-uraninite Products of
484   Microbial U(VI) Reduction. Environ. Sci. Technol. **2010,** 44 (24), 9456-9462.

485   (25)   Alessi, D. S.; Uster, B.; Veeramani, H.; Suvorova, E. I.; Lezama-Pacheco, J. S.; Stubbs,
486   J. E.; Bargar, J. R.; Bernier-Latmani, R., Quantitative separation of monomeric U(IV) from UO_2
487   in products of U(VI) reduction. Environ. Sci. Technol. **2012,** 46 (11), 6150-6157.

488   (26)   Yabusaki, S. B.; Fang, Y.; Long, P. E.; Resch, C. T.; Peacock, A. D.; Komlos, J.; Jaffe, P.
489   R.; Morrison, S. J.; Dayvault, R. D.; White, D. C.; Anderson, R. T., Uranium removal from
490   groundwater via in situ biostimulation: Field-scale modeling of transport and biological
491   processes. J. Contam. Hydrol. **2007,** 93 (1–4), 216-235.

492   (27)   Li, L.; Steefel, C. I.; Williams, K. H.; Wilkins, M. J.; Hubbard, S. S., Mineral
493   Transformation and Biomass Accumulation Associated With Uranium Bioremediation at Rifle,
494   Colorado. Environ. Sci. Technol. **2009,** 43 (14), 5429-5435.

495   (28)   Latta, D. E.; Gorski, C. A.; Boyanov, M. I.; O'Loughlin, E. J.; Kemner, K. M.; Scherer,
496   M. M., Influence of magnetite stoichiometry on U^{VI} reduction. Environ. Sci. Technol. **2012,** 46
497   (2), 778-786.

498   (29)   Veeramani, H.; Scheinost, A. C.; Monsegue, N.; Qafoku, N. P.; Kukkadapu, R.;
499   Newville, M.; Lanzirotti, A.; Pruden, A.; Murayama, M.; Hochella, M. F., Abiotic Reductive
500   Immobilization of U(VI) by Biogenic Mackinawite. Environ. Sci. Technol. **2013,** 47 (5), 2361-
501   2369.

502   (30)   Singer, D. M.; Chatman, S. M.; Ilton, E. S.; Rosso, K. M.; Banfield, J. F.; Waychunas, G.
503   A., Identification of simultaneous U(VI) sorption complexes and U(IV) nanoprecipitates on the
504   magnetite (111) surface. Environ. Sci. Technol. **2012**.

505   (31)   O'Loughlin, E. J.; Kelly, S. D.; Cook, R. E.; Csencsits, R.; Kemner, K. M., Reduction of
506   uranium(VI) by mixed iron(II)/iron(III) hydroxide (green rust): Formation of UO_2 nanoparticles.
507   Environ. Sci. Technol. **2003,** 37 (4), 721-727.

508   (32)   O'Loughlin, E. J.; Kelly, S. D.; Kemner, K. M., XAFS investigation of the interactions of
509   U^{VI} with secondary mineralization products from the bioreduction of Fe^{III} oxides. Environ. Sci.
510   Technol. **2010,** 44 (5), 1656-1661.

511   (33)   Latta, D. E.; Pearce, C. I.; Rosso, K. M.; Kemner, K. M.; Boyanov, M. I., Reaction of U^{VI}
512   with Titanium-Substituted Magnetite: Influence of Ti on U^{IV} Speciation. Environ. Sci. Technol.
513   **2013,** 47 (9), 4121-4130.

514   (34)   Gorski, C. A.; Scherer, M. M., Influence of magnetite stoichiometry on Fe^{II} uptake and
515   nitrobenzene reduction. Environ. Sci. Technol. **2009,** 43 (10), 3675-3680.

516   (35)   O'Loughlin, E. J., Effects of electron transfer mediators on the bioreduction of
517   lepidocrocite (gamma-FeOOH) by Shewanella putrefaciens CN32. Environ. Sci. Technol. **2008,**
518   42 (18), 6876-6882.

519   (36)   Garrett, R. G., Relative spatial soil geochemical variability along two transects across the
520   United States and Canada. Appl. Geochem. **2009,** 24 (8), 1405-1415.

521   (37)   Skomurski, F. N.; Ilton, E. S.; Engelhard, M. H.; Arey, B. W.; Rosso, K. M.,
522   Heterogeneous reduction of U^{6+} by structural Fe^{2+} from theory and experiment. Geochim.
523   Cosmochim. Acta **2011,** 75 (22), 7277-7290.

524   (38)   Ilton, E. S.; Boily, J.-F.; Buck, E. C.; Skomurski, F. N.; Rosso, K. M.; Cahill, C. L.;
525   Bargar, J. R.; Felmy, A. R., Influence of dynamical conditions on the reduction of U^{VI} at the
526   magnetite-solution interface. Environ. Sci. Technol. **2009,** 44 (1), 170-176.

527   (39)   Lee, S. Y.; Baik, M. H.; Choi, J. W., Biogenic formation and growth of uraninite (UO$_2$).
528   Environ. Sci. Technol. **2010,** 44 (22), 8409-8414.

529   (40)   Rui, X.; Kwon, M. J.; O'Loughlin, E. J.; Dunham-Cheatham, S.; Fein, J. B.; Bunker, B.;
530   Kemner, K. M.; Boyanov, M. I., Bioreduction of Hydrogen Uranyl Phosphate: Mechanisms and
531   U(IV) Products. Environ. Sci. Technol. **2013,** 47 (11), 5668-5678.

532   (41)   Wyckoff, R. W. G., Crystal Structures. Interscience: New York, 1960; Vol. 2.

533   (42)   Hennig, C.; Ikeda-Ohno, A.; Emmerling, F.; Kraus, W.; Bernhard, G., Comparative
534   investigation of the solution species [U(CO$_3$)$_5$]$^{6-}$ and the crystal structure of
535   Na$_6$[U(CO$_3$)$_5$]·12H$_2$O. Dalton Trans. **2010,** 39 (15), 3744-3750.

536   (43)   Hennig, C.; Kraus, W.; Emmerling, F.; Ikeda, A.; Scheinost, A. C., Coordination of a
537   Uranium(IV) Sulfate Monomer in an Aqueous Solution and in the Solid State. Inorg. Chem.
538   **2008,** 47 (5), 1634-1638.

539   (44)   Harris, W. E.; Kolthoff, I. M., The Polarography of Uranium. III. Polarography in Very
540   Weakly Acid, Neutral or Basic Solution1. J. Am. Chem. Soc. **1947,** 69 (2), 446-451.

541   (45)   Kern, D. M. H.; Orlemann, E. F., The Potential of the Uranium (V), Uranium (VI)
542   Couple and the Kinetics of Uranium (V) Disproportionation in Perchlorate Media. J. Am. Chem.
543   Soc. **1949,** 71 (6), 2102-2106.

544   (46)   Ilton, E. S.; Haiduc, A.; Cahill, C. L.; Felmy, A. R., Mica surfaces stabilize pentavalent
545   uranium. Inorg. Chem. **2005,** 44 (9), 2986-2988.

546   (47)   Boyanov, M. I.; O'Loughlin, E. J.; Roden, E. E.; Fein, J. B.; Kemner, K. M., Adsorption
547   of Fe(II) and U(VI) to carboxyl-functionalized microspheres: The influence of speciation on
548   uranyl reduction studied by titration and XAFS. Geochim. Cosmochim. Acta **2007,** 71 (8), 1898-
549   1912.

550   (48)   Müller, K.; Foerstendorf, H.; Meusel, T.; Brendler, V.; Lefèvre, G.; Comarmond, M. J.;
551   Payne, T. E., Sorption of U(VI) at the TiO2–water interface: An in situ vibrational spectroscopic
552   study. Geochim. Cosmochim. Acta **2012,** 76 (0), 191-205.

553   (49)   Latta, D. E.; Boyanov, M. I.; Kemner, K. M.; O'Loughlin, E. J.; Scherer, M. M., Abiotic
554   reduction of uranium by Fe(II) in soil. Appl. Geochem. **2012,** 27 (8), 1512-1524.

555   (50)   Cologgi, D. L.; Lampa-Pastirk, S.; Speers, A. M.; Kelly, S. D.; Reguera, G., Extracellular
556   reduction of uranium via Geobacter conductive pili as a protective cellular mechanism. Proc.
557   Natl. Acad. Sci. USA **2011,** 108 (37), 15248-15252.

558   (51)   Huber, F.; Schild, D.; Vitova, T.; Rothe, J.; Kirsch, R.; Schäfer, T., U(VI) removal
559   kinetics in presence of synthetic magnetite nanoparticles. Geochim. Cosmochim. Acta **2012,** 96,
560   154-173.

561

562